

# A Designer Scaffold with Immune Nanoconverters for Reverting Immunosuppression and Enhancing Immune Checkpoint Blockade Therapy

Hathaichanok Phuengkham, Chanyoung Song, and Yong Taik Lim\*

**Current cancer immunotherapy based on immune checkpoint blockade (ICB) still suffers from low response rate and systemic toxicity. To overcome the limitation, a novel therapeutic platform that can revert nonimmunogenic tumors into immunogenic phenotype is highly required. Herein, a designer scaffold loaded with both immune nanoconverters encapsulated with resiquimod (iNCVs (R848)) and doxorubicin, which provides the polarization of immunosuppressive tumor-associated macrophages (TAMs) and myeloid-derived suppressor cells (MDSCs) into tumoricidal antigen-presenting cells (APCs), rather than depleting them, as well as in situ vaccination that can be generated in vivo without the need to previously analyze and sequence tumor antigens to favor neoantigen-specific T cell responses is suggested. Local and sustained release of iNCVs (R848) and doxorubicin from the designer scaffold not only reduces the frequency of immunosuppressive cells in tumors but also increases systemic antitumor immune response, while minimizing systemic toxicity. Reshaping the tumor microenvironment (TME) using the designer-scaffold-induced synergistic antitumor immunity with ICB effects and long-term central and effector memory T cell responses, results in the prevention of postsurgical tumor recurrence and metastasis. The spatiotemporal modulation of TMEs through designer scaffolds is expected to be a strategy to overcome the limitations and improve the therapeutic efficacy of current immunotherapies with minimized systemic toxicity.**

response rate to ICB therapies, the promotion of an immunogenic tumor phenotype through a combination of cancer therapies that does not generate systemic toxicity is necessary.<sup>[3]</sup> In situ vaccination is a powerful cancer prevention strategy that can be generated in vivo without the need to previously analyze and sequence tumor antigens to favor neoantigen-specific T cell responses.<sup>[4]</sup> Several clinical studies have highlighted the promising effects of the combination of in situ vaccination and ICB treatment; however, most of these studies have been unsuccessful in significantly impacting the highly immunosuppressive tumor microenvironment (TME) in advanced-stage cancers or postsurgical treatment cancers.<sup>[5]</sup> Surgery is the most effective treatment regimen for patients with solid tumors, and half of all patients with cancer undergo surgery with a curative intent.<sup>[6]</sup> However, surgical procedures may induce immunosuppression owing to the generation of wound healing factors, which stimulate tumor recurrence and metastasis.<sup>[7]</sup> Inflammatory cells (such as tumor-associated macrophages (TAMs), myeloid-derived suppressor cells (MDSCs), etc.) and soluble mediators (such as trans-

forming growth factor beta (TGF- $\beta$ ), interleukin (IL)-10, etc.) have been found to accumulate to high levels in recurrent tumors and produce a remarkably suppressive environment to inhibit T cell activation and proliferation.<sup>[7b,8]</sup> Considering the marked changes in the postsurgical TME, a combination therapy that considers modulating immunosuppression may hold great promise in improving clinical outcomes. Furthermore, the polarization of immunosuppressive MDSCs and TAMs in the TME into tumor-suppressing cells would be a better strategy than inhibiting or depleting these immunosuppressive cells.<sup>[9]</sup> Resiquimod (R848) is an imidazoquinoline-based small-molecule compound that is recognized by Toll-like receptor (TLR) 7/8. It has been reported that the recognition of R848 in the endosome leads to the activation and maturation of antigen-presenting cells (APCs) and induces the secretion of proinflammatory cytokines, type I interferons (IFNs), and chemokines.<sup>[10]</sup> In addition to its immunostimulatory function, R848 can also modulate immunosuppressive cells such as MDSCs and M2 macrophages.<sup>[11]</sup> R848 can transform MDSCs into APCs, such as dendritic cells (DCs) and macrophages, and polarize TAMs from the M2 phenotype into the M1 phenotype.

Immune checkpoint blockade (ICB) therapy is a promising strategy that elicits durable antitumor responses against various malignant tumors; however, therapeutic efficacy is limited to 5–30% depending on the tumor type.<sup>[1]</sup> Researchers have observed that ICB treatment generally produces durable clinical responses only in tumors classified as “immunogenic phenotypes,” which are characterized by high T cell infiltration and neoantigen burden and low immunosuppression.<sup>[1a,2]</sup> To enhance the

Dr. H. Phuengkham, Dr. C. Song, Prof. Y. T. Lim  
Department of Nano Engineering  
SKKU Advanced Institute of Nanotechnology (SAINT)  
and School of Chemical Engineering  
Sungkyunkwan University (SKKU)  
2066 Seobu-ro, Jangan-gu, Suwon, Gyeonggi-do 16419  
Republic of Korea  
E-mail: yongtaik@skku.edu

 The ORCID identification number(s) for the author(s) of this article can be found under <https://doi.org/10.1002/adma.201903242>.

DOI: 10.1002/adma.201903242

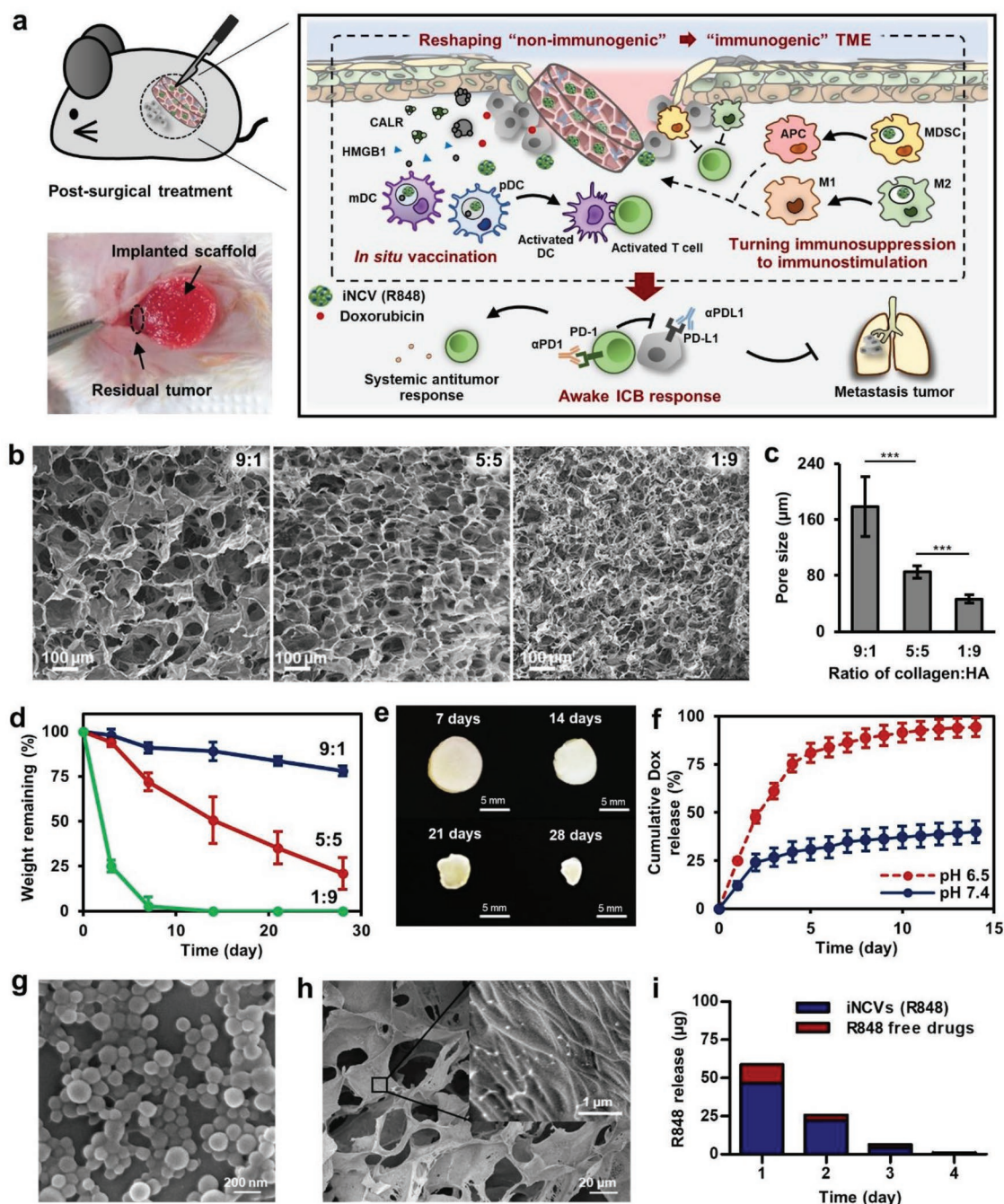


**Figure 1.** Schematic illustration and characterization of a designer scaffold for reverting immunosuppressive postsurgical TMEs and enhancing ICB treatment. a) Schematic diagram showing the design of a scaffold that codelivers iNCVs (R848), doxorubicin (Dox), and ICB molecules ( $\alpha$ PD1/ $\alpha$ PD1 antibodies) to induce an immunogenic tumor phenotype resulting in an enhanced ICB response. b) SEM analysis of the morphology and c) pore size of collagen/HA scaffolds prepared using different collagen:HA ratios. d) In vitro (1:9, 5:5, and 9:1) and e) in vivo degradation tests of the scaffold (5:5). f) In vitro profile of Dox release from the scaffold in an enzyme-containing buffer (pH 7.4 or 6.5). g) A representative SEM image of iNCVs (R848) and h) the iNCVs (R848)-loaded scaffold. i) In vitro release of iNCVs (R848) from the scaffold. Data are presented as the mean  $\pm$  S.D. ( $n = 3$ ).  $P$  values were determined by one-way ANOVA and Tukey's test ( $***P < 0.001$ ).

Here, we suggest a designer scaffold loaded with both immune nanoconverters (iNCVs) encapsulated with R848 (iNCVs (R848)) and doxorubicin, which can be applied to a postsurgical model for the spatiotemporal modulation of the nonimmunogenic TME into an immunogenic milieu, thereby

resulting in an increase in the therapeutic efficacy of ICB therapies (Figure 1a). Doxorubicin in the scaffold could turn the tumor into a self-vaccine site, where eradicated tumor cells serve as antigen sources to generate a host antitumor immune response, by mediating the immunogenic cell death (ICD) of

tumor cells. iNCVs (R848) could not only activate recruited APCs and induce antigen-specific T cells as vaccine adjuvants but also polarize MDSCs and TAMs into APCs, resulting in the reprogramming of the tumor into an immunogenic phenotype and the synergistic induction of antitumor immunity in combination with ICB therapies to prevent tumor recurrence and metastasis (Figure 1a). The immunotherapeutic efficacy of the designer scaffold was then investigated in 4T1 breast cancer and TC1 cervical cancer models.

Porous scaffolds were fabricated from a crosslinked collagen-hyaluronic acid (HA) matrix, which is widely used as a natural polymer for implantable matrices owing to its excellent biodegradability and biocompatibility.<sup>[12]</sup> The porous matrix was made by slowly freezing the polymer mixture, followed by lyophilization and crosslinking according to the method described in our previous study.<sup>[9]</sup> The morphology of the cross-section of the scaffold was examined by scanning electron microscopy (SEM), which showed a highly porous and interconnected structure that appeared to be relatively homogeneous throughout the bulk of the scaffold (Figure 1b). The pore size and degradation rate of the scaffold could be modulated depending on the initial mixture ratio of collagen and HA (Figure 1b–e; Figure S1, Supporting Information). The scaffold with a collagen to HA ratio of 5:5 (w/w) showed a uniform pore diameter size of 85  $\mu\text{m}$  and optimal in vitro and in vivo degradation rates over approximately one month. The scaffold could be incorporated with various therapeutics (such as small molecules, soluble proteins, nanoparticles, etc.) and fine-tuned to have a desirable release profile. Doxorubicin was loaded in the scaffold homogeneously by simple solution dropping followed by lyophilization for further use. To mimic the physiological condition of a tumor bed (an inflamed or a hypoxic TME), the in vitro release of doxorubicin from the scaffold was studied under acidic pH conditions ( $\approx\text{pH}$  6.5).<sup>[13]</sup> The encapsulated doxorubicin was released slowly from the scaffold in a buffer at pH 7.4 due to the strong hydrogen bonding and hydrophobic interactions between doxorubicin and the polymer matrix. On the other hand, the release of doxorubicin was triggered and sustained within two weeks in a buffer at pH 6.5 (Figure 1f). A possible explanation for these observations is that the amine groups of doxorubicin were protonated under the acidic condition, leading to weakening of the interaction between the hydrogen bonds and the subsequent release of the drug.<sup>[14]</sup>

The TLR7/8 agonist R848 induces antitumor immune responses by affecting the functions of immune cells, tumor cells, and the TME.<sup>[10b,c]</sup> TLR7/8 expression has been detected in various immune cells, including DCs, macrophages, and MDSCs.<sup>[15]</sup> As TLR7/8 exist in the endosomal compartment of cells, the delivery of R848 into cells is essential for the activation of immune cells. Thus, R848 was designed to be encapsulated in iNCVs made from biocompatible and biodegradable poly(lactic-co-glycolic acid) for efficient delivery. The formulation of iNCVs (R848) was optimized to achieve high drug loading with an iNCV size of  $\approx 100$  nm (Figure 1g; Table S1, Supporting Information). To assess the uptake efficiency of the iNCVs (R848), rhodamine was used as a model small-molecule payload for R848. As shown in Figure S2a of the Supporting Information, the efficiency of rhodamine uptake was higher after rhodamine was encapsulated in the iNCVs than when

it was in its free soluble form. Confocal microscopy images showed that iNCVs (rhodamine) were significantly accumulated inside cells and colocalized with LysoTracker (an endo/a lysosomal marker), suggesting the efficient delivery of R848 into the endo/lysosome (Figure S2b, Supporting Information). Prepared iNCVs (R848) were homogeneously loaded and showed a profile of sustained release from the scaffold within 3 days (Figure 1h,i). The release of R848 from the scaffold was mainly in form of iNCVs (R848) rather than free drug which offered the efficient delivery of R848 to the endosome part of immune cells (Figure 1i; Figure S3, Supporting Information).

The generation of an in situ cancer vaccine was preliminarily evaluated via an in vitro test. Aside from its conventional usage as a chemotherapeutic agent, doxorubicin is known to induce an immunological response through a special cancer-killing mechanism known as ICD.<sup>[16]</sup> Doxorubicin-induced selective cytotoxicity in 4T1 cancer cells (Figure 2a; Figure S4, Supporting Information) and rapid translocation of calreticulin (CALR) to the cell surface, as monitored by confocal microscopy and flow cytometry (Figure 2b,c). Surface exposure of CALR serves as an “eat me” signal to APCs, leading to immunogenic uptake of tumor antigens and the subsequent generation of antigen-specific T cell responses.<sup>[16,17]</sup> Dying cancer cells also release high-mobility group box 1 (HMGB1) as a “danger” signal that is recognized by TLR4 to induce APC maturation.<sup>[16,18]</sup> We observed a significant increase in HMGB1 release from the doxorubicin-treated 4T1 cells and upregulated expression of the CD80 surface activation marker on DCs after treatment with doxorubicin-treated 4T1 medium (Figure 2d,e). R848 is known to promote the maturation of APCs and enhance cellular immunity.<sup>[10]</sup> The immunostimulatory effect of iNCVs (R848) on APCs was investigated based on the upregulation of the expression of a surface activation marker and the secreted levels of proinflammatory cytokines. Treatment with soluble R848 or iNCVs (R848) significantly upregulated the expression of CD80 and promoted the secretion of IL-6, IL-12, and tumor necrosis factor (TNF)- $\alpha$  in both DCs and macrophages in a dose-dependent manner (Figure 2f,g). The upregulation of CD80 expression and the secretion of proinflammatory cytokines by the immune cells were much higher after treatment with iNCVs (R848) than after treatment with soluble R848, probably owing to the efficient delivery of R848 to the endosomes mediated by the nanoparticles. These data suggest the generation of an in situ cancer vaccine through the induction of multiple modalities of cell death in response to doxorubicin treatment and highlight the immunostimulatory effects of iNCVs (R848).

TAMs and MDSCs are the most abundant infiltrated myeloid cells in solid tumors that exert protumor functions in the TME.<sup>[11]</sup> Re-education of these immunosuppressive cells is critical to enhancing therapeutic effects and suppressing tumor growth. Recent studies have shown that TAMs and MDSCs respond to stimulation via a TLR7/8 agonist by differentiating into tumoricidal APCs, leading to the elimination of established cancers.<sup>[11]</sup> Thus, we investigated the polarizing effects of iNCVs (R848) on TAMs and MDSCs. In general, macrophages show notable plasticity in response to different environmental cues. These cells can switch between two main phenotypes, the antitumorigenic M1 phenotype and protumorigenic M2 phenotype, depending on surrounding signals.<sup>[19]</sup> We generated M1

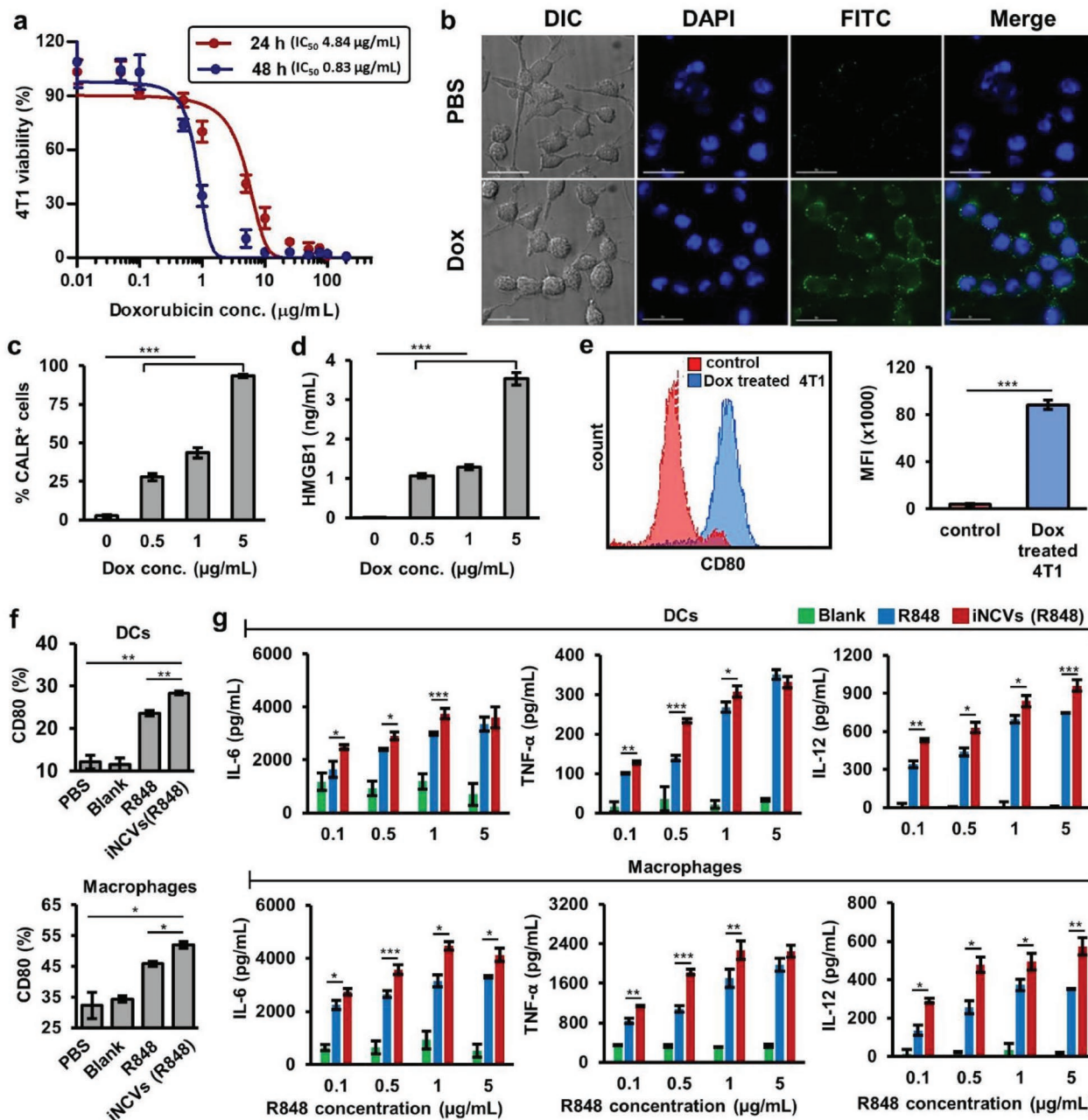


**Figure 2.** In vitro test of iNCVs (R848) and doxorubicin for the generation of in situ vaccine. a) Cell viability of 4T1 cells after treatment with various concentrations of doxorubicin measured by an MTS assay. b) Induction of immunogenic changes in 4T1 cells by doxorubicin treatment ( $1 \mu\text{g mL}^{-1}$ ). Representative fluorescence images showed the induction of CALR in 4T1 cells in the presence of doxorubicin for 4 h. Cell nuclei and CALR were detected with Hoechst and FITC-conjugated anti-CALR antibody staining, respectively. c) Flow cytometry analysis of CALR<sup>+</sup> 4T1 cells. d) Release of HMGB1 into the medium of doxorubicin-treated 4T1 cells examined 24 h after treatment using ELISA. e) Histograms representing the expression of cell surface activation markers on DCs following treatment with doxorubicin-treated 4T1 cell medium ( $1 \mu\text{g mL}^{-1}$ ). f) Flow cytometry analysis of the expression of surface activation markers on DCs and macrophages. g) Quantification of cytokine production via ELISA following treatment with PBS, empty iNCVs (blank), R848, or iNCVs (R848). Data are presented as the mean  $\pm$  S.D. ( $n = 3$ ).  $P$  values were determined by Student's  $t$ -test and one-way ANOVA with Tukey's test (\* $P < 0.05$ , \*\* $P < 0.01$ , and \*\*\* $P < 0.001$ ).

and M2 macrophages in vitro from RAW 264.7 cells (M0) using lipopolysaccharide or IL-4 stimulation, respectively, and these phenotypes were confirmed by assessing the upregulation of surface marker expression and cytokine secretion (Figure S5, Supporting Information).<sup>[20]</sup> M1 macrophages showed upregulated CD86 expression and secretion of proinflammatory

cytokines (TNF- $\alpha$ , IL-6, and IL-12) and nitric oxide (NO), while M2 macrophages showed upregulated expression of CD206 and secreted high levels of an anti-inflammatory cytokine (IL-10) as well as arginase-1 (Arg) (Figure S5, Supporting Information). The M2 macrophages that closely resembled TAMs were used for in vitro testing. When the M2 macrophages were incubated

with iNCVs (R848), a marked increase in the M1 marker level was observed, and this level was significantly higher than that observed following treatment with soluble R848 (Figure 3a–c). The ability of iNCVs (R848) to convert MDSCs into mature APCs with tumoricidal activity was also investigated (Figure 3d,e). Purified MDSCs cultured in the presence of iNCVs (R848) showed significantly upregulated expression of DC-associated (CD11c<sup>+</sup>) and macrophage-associated (F4/80<sup>+</sup>) surface markers. Treatment with iNCVs (R848) also promoted the secretion of the proinflammatory cytokines IL-12 and IL-6. These results are consistent with the results reported in an earlier finding, wherein R848 induced the differentiation of TAMs and MDSCs into tumoricidal APCs and was shown to be remarkably efficient upon encapsulation in nanoparticles.

Then, we tested the efficacy of the designer scaffold loaded with iNCVs (R848) and doxorubicin as a postoperative treatment in an advanced-stage primary 4T1 breast tumor model which demonstrated a poorly immunogenic TME (Figure S6, Supporting Information). Surgery was performed as shown in Figure S7 of the Supporting Information by removing ~90% of the established primary tumor. Mice with the same tumor size underwent the surgical intervention, and those with the same size residual tumors were carefully selected for further experiments (Figure S8, Supporting Information). All mice treated only with surgery showed tumor relapse and metastasis, resulting in death within 28 days (Figure 4a–c; Figure S9, Supporting Information). Compared to treatment with scaffold containing iNCVs (R848) or doxorubicin alone or a bolus

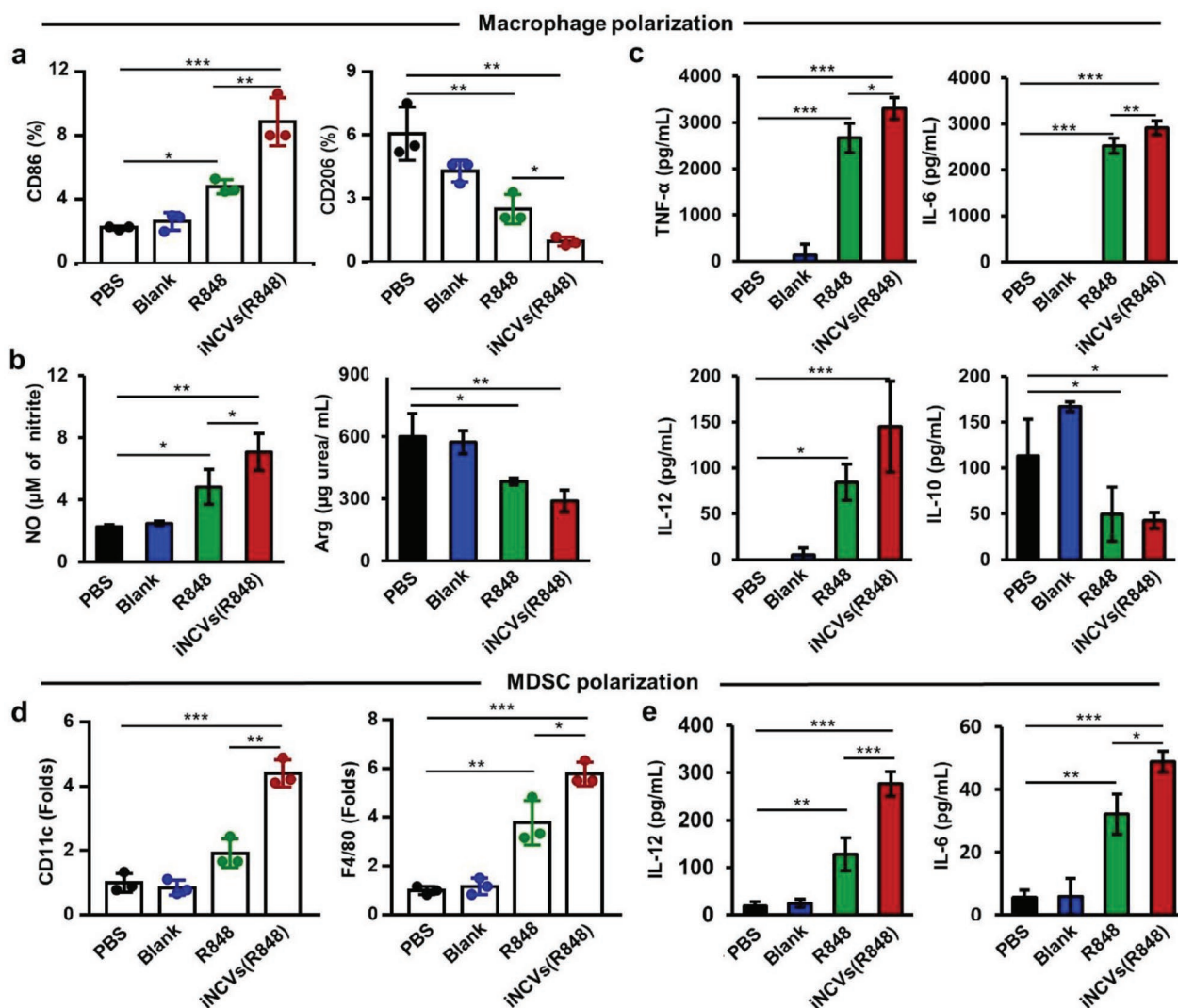


**Figure 3.** iNCVs (R848) turned immunosuppressive myeloid cells into tumoricidal APCs. a–c) iNCVs (R848) induced the polarization of M2 macrophages into M1 macrophages. M2 macrophages were incubated with PBS, empty iNCVs (blank), R848, or iNCVs (R848) ( $5 \mu\text{g mL}^{-1}$  of R848) for 24 h. Polarization was analyzed by assessing: a) the expression of surface markers (CD86 and CD206), b) the production of Arg and NO production, and c) the secretion of cytokines (TNF- $\alpha$ , IL-6, IL-12, and IL-10). d,e) iNCVs (R848) induced the polarization of MDSCs into tumoricidal APCs. d) Flow cytometry was used to analyze surface markers associated with DCs (CD11c<sup>+</sup>) and macrophages (F4/80<sup>+</sup>). e) The production of the proinflammatory cytokines IL-12 and IL-6 was analyzed by ELISA. Data are presented as the mean  $\pm$  S.D. ( $n = 3$ ).  $P$  values were determined by one-way ANOVA and Tukey's test (\* $P < 0.05$ , \*\* $P < 0.01$ , and \*\*\* $P < 0.001$ ).

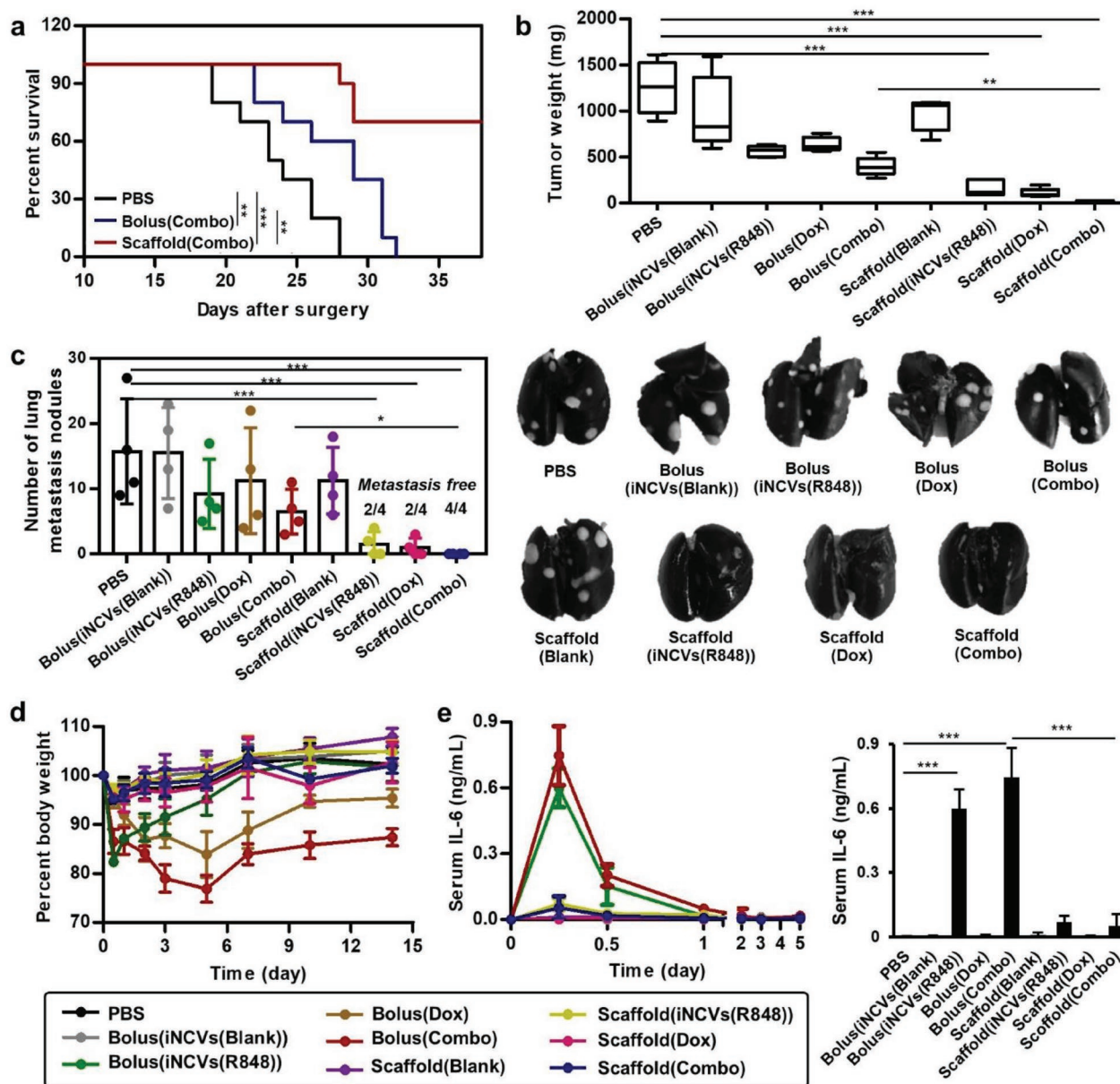


**Figure 4.** Spatiotemporal delivery of therapeutics via the designer scaffold enhances therapeutic efficiency and reduces systemic toxicity. a) Survival rate of mice after treatment. Tumors were treated with surgery (10% of the tumor remained) at 14 days after inoculation and subsequently treated as follows: PBS, soluble empty iNCVs (bolus(iNCVs(blank))), soluble iNCVs (R848) (bolus(iNCVs(R848))), soluble doxorubicin (bolus(Dox)), soluble of both (bolus(combo)), empty scaffold (scaffold(blank)), iNCVs(R848)-loaded scaffold (scaffold(iNCVs (R848))), doxorubicin-loaded scaffold (scaffold(Dox)), or scaffold loaded with both (scaffold(combo)). Doxorubicin and R848 were treated with the same dose at 200 and 100  $\mu\text{g}$ , respectively. Differences in survival were determined for each group by the Kaplan–Meier method, and the overall  $P$  value was calculated by the log-rank test ( $n = 10$ ). b) Tumor weight ( $n = 5$ ) and c) number of metastatic lung nodules ( $n = 4$ ) and representative images of the lungs collected from mice at 14 days after treatment. White nodules indicate metastatic tumors in the lungs. d) Percent body weight change and e) serum levels of IL-6 following administration of different treatments to assess toxicity ( $n = 5$ ).  $P$  values were determined by one-way ANOVA and Tukey's test ( $*P < 0.05$ ,  $**P < 0.01$ , and  $***P < 0.001$ ).

injection, treatment with scaffold containing both iNCVs (R848) and doxorubicin synergistically inhibited tumor recurrence and metastasis, resulting in prolonged survival. Notably, local treatment with the scaffold could generate a systemic antitumor immune response and inhibit tumor growth on distal lesions (Figure S10, Supporting Information).

In fact, doxorubicin treatments are greatly limited by extensive side effects mainly due to the toxicity of the drugs on normal

tissues.<sup>[21]</sup> In addition, to date, only a few immunomodulators have been approved as adjuvants in FDA-licensed vaccines, and several molecules have failed to enter clinical practice despite a multitude of promising results obtained in preclinical studies.<sup>[22]</sup> These failures are attributed to the imbalance between immunogenicity generation and safety concerns, leading to the induction of systemic inflammatory responses. It is important to spatiotemporally control the delivery of

encapsulated substances to tumor sites without generating any undesirable side effects. Thus, in addition to the analysis of antitumor activity, we also evaluated the systemic toxicity of this delivery platform. Upon local treatment, bolus administration of iNCVs (R848), doxorubicin, and combo resulted in substantial weight loss in mice, and 10%, 30%, and 40% of the mice died, respectively (Figure 4d). In addition, bolus administration of iNCVs (R848) and combo caused a marked increase in the serum level of IL-6 within 6 h (Figure 4e). These results may be associated with the rapid diffusion of the iNCVs (R848) bolus from the surgical site causing inflammatory effects. By contrast, compared with phosphate-buffered saline (PBS) treatment, treatment of mice with the scaffold platform produced

no significant weight loss at any time point. These results confirmed the potential benefits of the scaffold as a reservoir for controlling the release of immunomodulators to enhance therapeutic efficacy and avoid systemic side effects.

To investigate the cellular and molecular changes among immune cell subsets after treatment with the scaffold by each therapeutic, infiltrating immune cells and cytokine production in the tumor and lymphoid organs were analyzed seven days after treatment. The combination treatment significantly enhanced the infiltration of immune effector cells (CD4<sup>+</sup> and CD8<sup>+</sup> T cells and M1 macrophages) and reduced the frequency of immunosuppressive cells (MDSCs and M2 macrophages) in tumors (Figure 5a; Figure S11, Supporting Information).

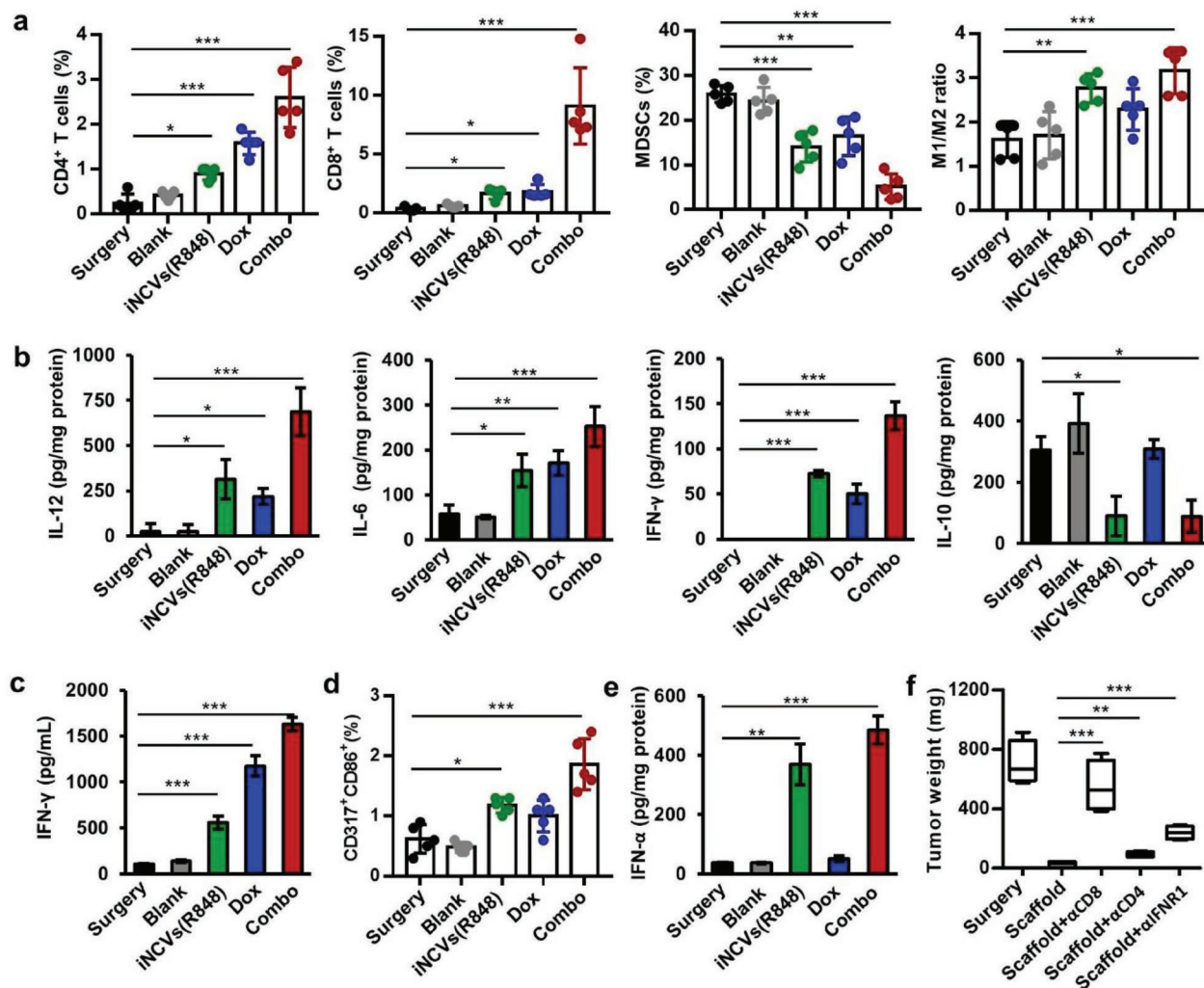


**Figure 5.** Antitumor effects of the designer scaffold are mediated by the reversion of the immunosuppressive microenvironment and the restoration of immunostimulation. Tumors were treated with surgery (10% of the tumor remained) at 14 days after inoculation and then treated with no further treatment (surgery), a blank scaffold (blank), iNCVs (R848)-loaded scaffold (iNCVs (R848)), a Dox-loaded scaffold (Dox), or a scaffold loaded with both (combo). a) Fluorescence-activated cell sorting analysis demonstrating the infiltration of CD4<sup>+</sup> and CD8<sup>+</sup> T cells (gated on CD3<sup>+</sup> cells), MDSCs (Gr1<sup>+</sup>CD11b<sup>+</sup>), and M1/M2 macrophages (ratio of MHCII<sup>+</sup> cells to CD206<sup>+</sup> cells within the gated F4/80<sup>+</sup> cell population) into the recurrent tumor at 7 days postsurgery. b) Cytokine levels in the recurrent tumor analyzed by ELISA. c) Antigen-specific response. Splenocytes were stimulated with 4T1 tumor antigen for 72 h. After incubation, the supernatants were collected and analyzed by ELISA. d) Fluorescence-activated cell sorting analysis demonstrating the infiltration of activated pDCs (CD317<sup>+</sup>CD86<sup>+</sup>) and e) type I IFN secretion (IFN-α) in the tumor-draining lymph node. f) Weight of the recurrent tumor after treatment with the scaffold containing iNCVs (R848) and doxorubicin (scaffold) when specific immune cell subsets were depleted to reveal their relative contributions. Data are presented as the mean ± S.D. (*n* = 5). *P* values were determined by one-way ANOVA and Tukey's test (\**P* < 0.05, \*\**P* < 0.01, and \*\*\**P* < 0.001).

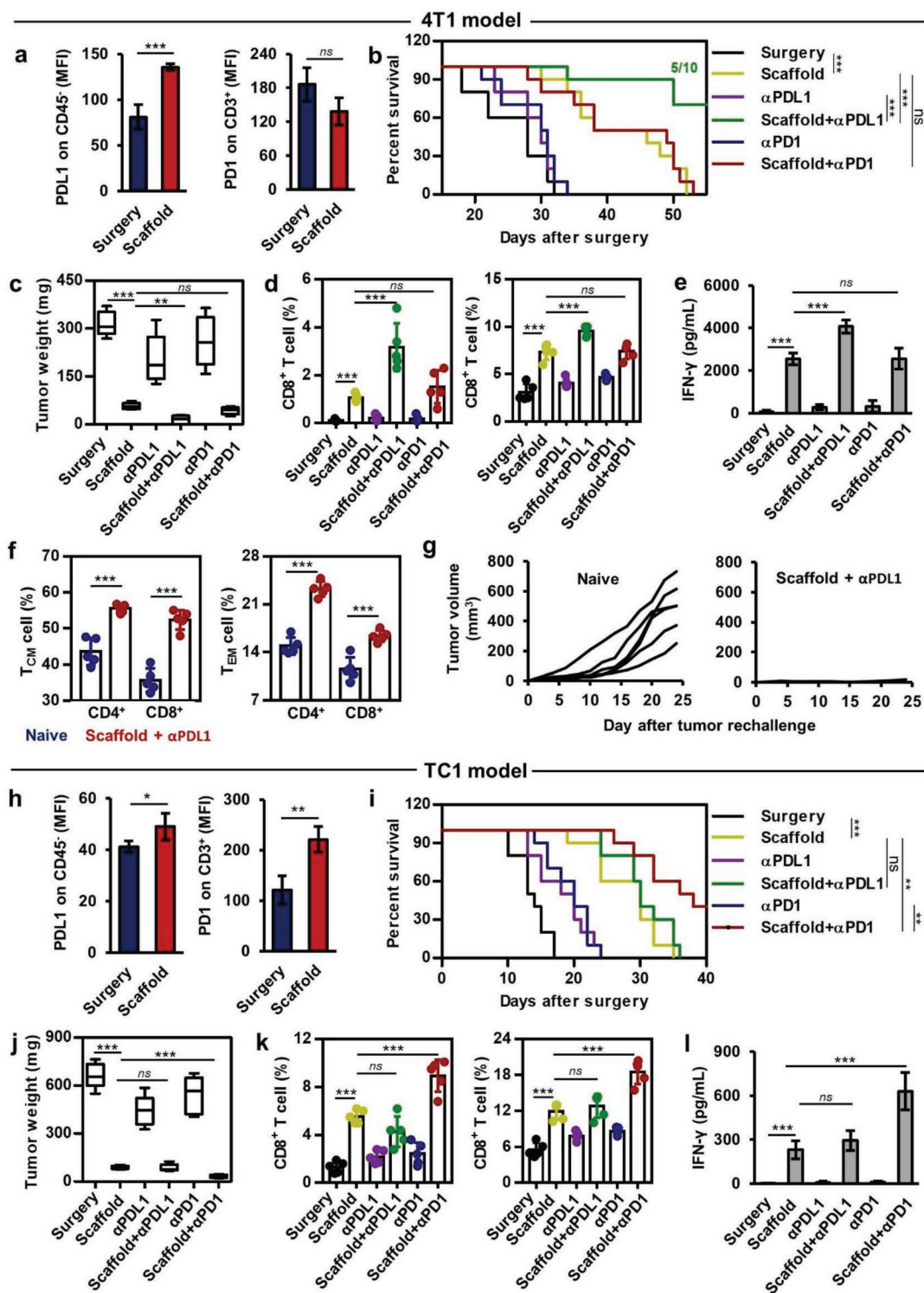


**Figure 6.** a–l) The designer scaffold enhances the therapeutic response to ICB therapies in postsurgical 4T1 (a–g) and TC1 models (h–l). a, h) Expression of PD-L1 and PD-1 in recurrent tumors after the scaffold (iNCVs (R848) + Dox) treatment ( $n = 5$ ). b, i) Survival curves after combination treatment with checkpoint inhibitors. Differences in survival were determined for each group by the Kaplan–Meier method, and the overall  $P$  value was calculated by the log-rank test ( $n = 10$ ). c, j) Recurrent tumor weight at day 7 after treatment. d, k) Infiltrating  $CD8^+$  T cells in the tumor (left) and spleen (right). e, l)  $IFN-\gamma$  secretion from activated T cells after combination treatment with checkpoint inhibitors. f) Quantitative analysis of memory T cells. Splenocytes isolated from tumor-free mice (treatment with scaffold +  $\alpha$ PDL1 antibody) and naive mice were analyzed for the presence of central memory T ( $T_{CM}$ ) cells and effector memory T ( $T_{EM}$ ) cells gated on  $CD4^+$  and  $CD8^+$  cells on day 40 immediately before rechallenging the mice with secondary tumors ( $n = 5$ ). g) Tumor volumes of naive and tumor-free mice (Scaffold +  $\alpha$ PDL1 treatment) post tumor-rechallenge ( $n = 6$ ). Data are presented as the mean  $\pm$  S.D.  $P$  values were determined by Student's  $t$ -test and one-way ANOVA with Tukey's test (\* $P < 0.05$ , \*\* $P < 0.01$ , and \*\*\* $P < 0.001$ ).

In addition, the localized release of the therapeutics also led to an increase in the percentage of T cells and a decrease in the percentage of MDSCs in the spleen (Figure S12, Supporting Information). Consistent with the immune profile, upregulated production of proinflammatory cytokines (IL-12, IL-6, and IFN- $\gamma$ ) and downregulated levels of immunosuppressive cytokines (IL-10) were observed in recurrent tumors after the combination treatment (Figure 5b). We assessed whether the inhibition of tumor recurrence and metastasis after scaffold implantation was related to the tumor antigen-specific T cell response by isolating splenocytes and restimulating them *ex vivo* with a 4T1 tumor lysate. The level of IFN- $\gamma$  production was increased in the combination treatment group, thereby confirming that antitumor immunity was mediated in an antigen-specific manner (Figure 5c). The combination treatment remarkably increased the percentage of activated DCs and upregulated the secretion of proinflammatory cytokines (IL-6 and IL-12) in the tumor-draining lymph nodes (Figure S13, Supporting Information). In addition, the levels of activated plasmacytoid DCs (pDCs) and type I IFNs (IFN- $\alpha$ ) were significantly increased after treatment with iNCVs (R848) or the combination regimen (Figure 5d,e). R848 is known to activate pDCs, which produce large amounts of type I IFNs.<sup>[10b,c]</sup> pDC-derived type I IFNs link the innate and adaptive immune responses in virus infection by stimulating antigen cross-presentation to T cells and directly inducing the differentiation of naïve T cells into T helper 1 (Th1) cells.<sup>[23]</sup> To understand the underlying *in vivo* antitumor mechanism of designer scaffold (iNCVs (R848) and doxorubicin) treatment, the roles of effector T cells and type I IFN signaling in the scaffold-mediated immune response were investigated by an antibody depletion test. Depleting either CD4<sup>+</sup> or CD8<sup>+</sup> T cells or neutralizing IFN- $\alpha/\beta$  receptor 1 caused a significant increase in tumor progression, implying that both T cell populations and type I IFN signaling were necessary for the inhibition of tumor recurrence (Figure 5f; Figure S14, Supporting Information).

The efficacy of the designer scaffold (iNCVs (R848) and doxorubicin) in reshaping the TME to enhance the response to ICB therapy was then investigated in two different tumor models, 4T1 breast cancer and TC1 cervical cancer models (Figure 6). Previous studies have shown that low-dose local administration of ICB antibodies is as effective as high-dose systemic administration but avoids the overstimulation of self-reactive T cells.<sup>[24]</sup> Anti-PD-L1 ( $\alpha$ PDL1, clone 10F.9G2) or anti-PD-1 ( $\alpha$ PD1, clone RMP1-14) antibodies were directly loaded into the scaffold, and sustained release was observed over 5 days (Figure S15, Supporting Information). After local implantation of the designer scaffold (iNCVs (R848) and doxorubicin), the upregulation of PD-L1/PD-1 expression in the TME was observed. A major increase in PD-L1 expression on tumor cells was observed in the 4T1 model, and PD-1 expression on T cells was observed in the TC1 model after scaffold (iNCVs (R848) and doxorubicin) treatment (Figure 6a,h). As previous studies have shown that chemotherapy remarkably increases the expression of immune checkpoint molecules in tumor tissue, the different upregulation patterns of PD-L1 and PD-1 expression in the different tumor models may be related to the different TME conditions in each tumor model in response to doxorubicin and iNCV (R848) treatment.<sup>[25]</sup> Upon the upregulation of PD-L1

expression in the 4T1 model and PD-1 expression in the TC1 model, the synergistic effect of the  $\alpha$ PDL1/ $\alpha$ PD1 antibodies and the designer scaffold (iNCVs (R848) and doxorubicin) was observed according to the tumor cell type, while treatment with the  $\alpha$ PDL1 or  $\alpha$ PD1 antibodies alone did not result in any enhanced antitumor effects on either tumor model. In the 4T1 tumors, the synergy of the designer scaffold (iNCVs (R848) and doxorubicin) and  $\alpha$ PDL1 antibodies led to the inhibition of tumor recurrence and a 100% prolonged mouse survival rate over a month (Figure 6b,c), while no effect was observed in the TC1 tumors. Remarkably, this synergistic effect also resulted in 50% of the mice being tumor free. The proportions of different T cell phenotypes in the spleen of these tumor-free mice were analyzed, which showed higher percentages of central memory T cells (CD44<sup>+</sup>CD62L<sup>+</sup>) and effector memory T cells (CD44<sup>+</sup>CD62L<sup>-</sup>) in the tumor-free mice than in naïve mice (Figure 6f; Figure S16, Supporting Information). To investigate the potent memory antitumor response, the tumor-free mice were reinoculated with 4T1 cells on the flank contralateral to the surgical site 40 days after tumor resection and treatment. Tumor growth in the treated mice (Scaffold +  $\alpha$ PDL1) was significantly inhibited, while continuous tumor growth was observed in naïve mice (Figure 6g). By contrast, the synergistic effect of the scaffold (iNCVs (R848) and doxorubicin) and  $\alpha$ PD1 antibody was distinctive in the TC1 tumors (Figure 6i,j). To understand these diverse response behaviors, the level of CD8<sup>+</sup> T cells in the tumor and spleen (Figure 6d,k) and the secretion of IFN- $\gamma$  by activated T cells (Figure 6e,l) after treatment with the different combinations were analyzed in the 4T1 and TC1 tumor models and showed trends consistent with the previous results. These results suggest that spatiotemporal TME modulation by implanting the designer scaffold could transform ICB-nonresponding tumors into responding ones. Although the  $\alpha$ PDL1 and  $\alpha$ PD1 antibodies target different cells, they both play a fundamental role in blocking the PD-L1/PD-1 axis. The different responses between the two antibodies may be related to the different location of target cells. The  $\alpha$ PDL1 antibody targeted cancer cells, and its impact is localized, which is mainly to alter the TME. By contrast, the  $\alpha$ PD1 antibody targets T cells, and its impact is systematic which would exert complex and multifunctional effects on both T cells and whole immune system.<sup>[25]</sup> The treatment of designer scaffold in TME is also expected to evoke different impacts on tumor cells and T cells, respectively, which are related to the different responses to  $\alpha$ PDL1 and  $\alpha$ PD1. In addition, further studies should be conducted systematically to understand the different responses to  $\alpha$ PD1 and  $\alpha$ PDL1 antibodies in different tumor models. However, we can speculate that they may be related to the different resistance mechanisms to checkpoint therapy depending on different TME condition in two tumor models.<sup>[26]</sup> Actually, several research groups are developing sets of biomarkers (PD-1/-L1 overexpression, mutational burden, tumor-infiltrating immune cells, and tumor environmental metabolites) associated with resistance and response to ICB. These studies can be helpful not only to disclose the underlying mechanism of the different responses to ICB in different tumors but also to guide optimal combination of immune modulators and ICB therapy in the clinic.<sup>[27]</sup>

In summary, we have developed a designer scaffold for the spatiotemporal delivery of immunotherapeutic agents to prevent

tumor recurrence and metastasis after the removal of large established primary tumors. The spatiotemporal release of doxorubicin from the scaffold triggered robust expression of signals associated with ICD and elicited an antigen-specific T cell response. iNCVs (R848) could act as adjuvants to activate innate immune cells as well as immunomodulators to reprogram immunosuppressive cells (TAMs and MDSCs) into tumoricidal APCs. The synergistic action of the TAM- and MDSC-repolarizing agents, which could convert the immunosuppressive TME into one that supports antitumor immunity, and the in situ cancer vaccine, which could elicit tumor antigen-specific T cell responses, resulted in the induction of systemic antitumor immunity. Although ICB therapies have been developed as potent alternatives to conventional treatment, their therapeutic efficacy is limited to only a small group of patients, and the systemic administration of these antibodies is still restricted by various side effects and resistance. The combined delivery of doxorubicin and iNCVs (R848) mediated by the scaffold elicited immunogenic phenotypes in tumors and changed  $\alpha$ PDL1/ $\alpha$ PD1-nonresponsive tumors into responsive tumors, resulting in significant increases in survival, the number of tumor-free mice, and the long-term memory T cell response. This strategy holds great promise for treating patients with poorly immunogenic tumors that are less responsive to ICB treatment. Moreover, local immunomodulation of the TME by the scaffold is a more specific, more effective, and less toxic therapeutic strategy for generating anticancer immunity than is bolus injection. Combination therapy generally increases the risk of side effects; however, we did not observe any obvious toxicity in the mice treated with the drug-loaded scaffolds. The designer scaffold we proposed herein may serve as a novel platform in cancer immunotherapy for the inhibition of tumor recurrence and metastasis.

## Supporting Information

Supporting Information is available from the Wiley Online Library or from the author.

## Acknowledgements

This work was supported by the National Research Foundation of Korea (NRF) grant funded by the Korean government (Grant Nos. 2017R1A2A1A17069277, 2017R1A5A1014560, and 2018M3A9H4078701). Animal studies were reviewed and approved by the Institutional Animal Care and Use Committee of Sungkyunkwan University School of Medicine, which is accredited by the Association for Assessment and Accreditation of Laboratory Animal Care International and abides by the Institute of Laboratory Animal Resources guide.

## Conflict of Interest

The authors declare no conflict of interest.

## Keywords

designer scaffolds, immune checkpoint inhibitor, immunotherapy, local immunization, tumor microenvironment

Received: May 21, 2019

Revised: August 19, 2019

Published online: September 6, 2019

- [1] a) P. Sharma, J. P. Allison, *Science* **2015**, *348*, 56; b) L. A. Emens, P. A. Ascierto, P. K. Darcy, S. Demaria, A. M. M. Eggermont, W. L. Redmond, B. Seliger, F. M. Marincola, *Eur. J. Cancer* **2017**, *81*, 116; c) A. Ribas, J. D. Wolchok, *Science* **2018**, *359*, 1350.
- [2] a) W. Zou, J. D. Wolchok, L. Chen, *Sci. Transl. Med.* **2016**, *8*, 328rv4; b) J. Galon, D. Bruni, *Nat. Rev. Drug Discovery* **2019**, *18*, 197.
- [3] a) C. Wang, J. Wang, X. Zhang, S. Yu, D. Wen, Q. Hu, Y. Ye, *Sci. Transl. Med.* **2018**, *10*, eaan3682; b) F. Dammeijer, S. P. Lau, C. H. J. van Eijck, S. H. van der Burg, J. G. J. V. Aerts, *Cytokine Growth Factor Rev.* **2017**, *36*, 5; c) H. Phuengkham, L. Ren, I. W. Shin, Y. T. Lim, *Adv. Mater.* **2019**, *31*, 1803322.
- [4] a) T. N. Schumacher, R. D. Schreiber, *Science* **2015**, *348*, 69; b) L. Hammerich, A. Binder, J. D. Brody, *Mol. Oncol.* **2015**, *9*, 1966.
- [5] a) L. Hammerich, T. A. Davis, T. Keler, A. M. Salazar, J. Brody, *Blood* **2016**, *128*, 465; b) L. Hammerich, M. Dhainaut, T. Keler, T. Davis, A. M. Salazar, B. D. Brown, J. D. Brody, *J. Immunol.* **2018**, *200*, 17.
- [6] J. C. Coffey, J. H. Wang, M. J. F. Smith, D. Bouchier-Hayes, T. G. Cotter, H. P. Redmond, *Lancet Oncol.* **2003**, *4*, 760.
- [7] a) B. V. Hogan, M. B. Peter, H. G. Shenoy, K. Horgan, T. A. Hughes, *Surgeon* **2011**, *9*, 38; b) J. Predina, E. Eruslanov, B. Judy, V. Kapoor, G. Cheng, L.-C. Wang, J. Sun, E. K. Moon, Z. G. Fridlender, S. Albelda, S. Singhal, *Proc. Natl. Acad. Sci. USA* **2013**, *110*, E415.
- [8] G. J. Szebeni, C. Vizler, L. I. Nagy, K. Kitajka, L. G. Puskas, *Int. J. Mol. Sci.* **2016**, *17*, 1958.
- [9] H. Phuengkham, C. Song, S. H. Um, Y. T. Lim, *Adv. Mater.* **2018**, *30*, 1706719.
- [10] a) M. Jurk, F. Heil, J. Vollmer, C. Schetter, A. M. Krieg, H. Wagner, G. Lipford, S. Bauer, *Nat. Immunol.* **2002**, *3*, 499; b) E. L. Smits, P. Ponsaerts, Z. N. Berneman, V. F. Van Tendeloo, *Oncologist* **2008**, *13*, 859; c) A. M. Krieg, J. Vollmer, *Immunol. Rev.* **2007**, *220*, 251.
- [11] a) C. B. Rodell, S. P. Arlauckas, M. F. Cuccarese, C. S. Garris, R. Li, M. S. Ahmed, R. H. Kohler, M. J. Pittet, R. Weissleder, *Nat. Biomed. Eng.* **2018**, *2*, 578; b) J. Wang, Y. Shirota, D. Bayik, H. Shirota, D. Tross, J. L. Gulley, L. V. Wood, J. A. Berzofsky, D. M. Klinman, *J. Immunol.* **2015**, *194*, 4215; c) D. Bayik, D. Tross, D. M. Klinman, *Front. Immunol.* **2018**, *9*, 608.
- [12] a) S. N. Park, H. J. Lee, K. H. Lee, H. Suh, *Biomaterials* **2003**, *24*, 1631; b) R. DeVolder, H. J. Kong, *Wiley Interdiscip. Rev.: Syst. Biol. Med.* **2012**, *4*, 351.
- [13] Y. Lu, A. A. Aimetti, R. Langer, Z. Gu, *Nat. Rev. Mater.* **2017**, *2*, 16075.
- [14] H. Wang, W. Gu, N. Xiao, L. Ye, Q. Xu, *Int. J. Nanomed.* **2014**, *9*, 1433.
- [15] Y. Shirota, H. Shirota, D. M. Klinman, *J. Immunol.* **2012**, *188*, 1592.
- [16] a) D. V. Krysko, A. D. Garg, A. Kaczmarek, O. Krysko, P. Agostinis, P. Vandenabeele, *Nat. Rev. Cancer* **2012**, *12*, 860; b) G. Kroemer, L. Galluzzi, O. Kepp, L. Zitvogel, *Annu. Rev. Immunol.* **2013**, *31*, 51.
- [17] M. Obeid, A. Tesniere, F. Ghiringhelli, G. M. Fimia, L. Apetoh, J. L. Perfettini, M. Castedo, G. Mignot, T. Panaretakis, N. Casares, D. Metivier, N. Larochette, P. van Endert, F. Ciccocanti, M. Piacentini, L. Zitvogel, G. Kroemer, *Nat. Med.* **2007**, *13*, 54.
- [18] L. Apetoh, F. Ghiringhelli, A. Tesniere, M. Obeid, C. Ortiz, A. Criollo, G. Mignot, M. C. Maiuri, E. Ullrich, P. Saulnier, H. Yang, S. Amigorena, B. Ryffel, F. J. Barrat, P. Saftig, F. Levi, R. Lidereau, C. Nogues, J. P. Mira, A. Chompret, V. Joulin, F. Clavel-Chapelon, J. Bourhis, F. Andre, S. Delaloge, T. Tursz, G. Kroemer, L. Zitvogel, *Nat. Med.* **2007**, *13*, 1050.
- [19] A. Mantovani, F. Marchesi, A. Malesci, L. Laghi, P. Allavena, *Nat. Rev. Clin. Oncol.* **2017**, *14*, 399.
- [20] H. L. Herd, K. T. Bartlett, J. A. Gustafson, L. D. McGill, H. Ghandehari, *Biomaterials* **2015**, *53*, 574.
- [21] P. K. Singal, N. Iliskovic, *N. Engl. J. Med.* **1998**, *339*, 900.
- [22] D. M. Harper, *Expert Rev. Vaccines* **2009**, *8*, 1663.
- [23] J. J. O'Shea, R. Visconti, *Nat. Immunol.* **2000**, *1*, 17.

- [24] M. F. Fransen, T. C. Van Der Sluis, F. Ossendorp, R. Arens, C. J. M. Melief, *Clin. Cancer Res.* **2013**, *19*, 5381.
- [25] a) K. E. Yost, A. T. Satpathy, D. K. Wells, Y. Qi, C. Wang, R. Kageyama, K. L. McNamara, J. M. Granja, K. Y. Sarin, R. A. Brown, R. K. Gupta, C. Curtis, S. L. Bucktrout, M. M. Davis, A. L. S. Chang, H. Y. Chang, *Nat. Med.* **2019**, *25*, 1251; b) J. Wei, C. Luo, Y. Wang, Y. Guo, H. Dai, C. Tong, D. Ti, Z. Wu, W. Han, *J. Immunother. Cancer* **2019**, *7*, 209.
- [26] a) P. Zhang, D.-M. Su, M. Liang, J. Fu, *Mol. Immunol.* **2008**, *45*, 1470; b) N. McGranahan, A. J. S. Furness, R. Rosenthal, S. Ramskov, R. Lyngaa, S. K. Saini, M. Jamal-Hanjani, G. A. Wilson, N. J. Birkbak, C. T. Hiley, T. B. K. Watkins, S. Shafi, N. Murugaesu, R. Mitter, A. U. Akarca, J. Linares, T. Marafioti, J. Y. Henry, E. M. Van Allen, D. Miao, B. Schilling, D. Schadendorf, L. A. Garraway, V. Makarov, N. A. Rizvi, A. Snyder, M. D. Hellmann, T. Merghoub, J. D. Wolchok, S. A. Shukla, C. J. Wu, K. S. Peggs, T. A. Chan, S. R. Hadrup, S. A. Quezada, C. Swanton, *Science* **2016**, *351*, 1463.
- [27] a) J. M. Pitt, M. Vetizou, R. Daillere, M. P. Roberti, T. Yamazaki, B. Routy, P. Lepage, I. G. Boneca, M. Chamillard, G. Kroemer, L. Zitvogel, *Immunity* **2016**, *44*, 1255; b) R. W. Jenkins, D. A. Barbie, K. T. Flaherty, *Br. J. Cancer* **2018**, *118*, 9.